Supporting Information

3D-Printed Hygroscopic Matrices Based on Granular Hydrogels for Atmospheric Water Adsorption and On-Demand Defogging

Xiaochun Wu, *Suxu Wang*, *Jun Zhao*, *Jingjing Li*, *Yuke Sun*, *Zhihang Wang**, *Petri Murto*, *Hongzhi Cui** & *Xiaofeng Xu**

X. Wu, S. Wang, J. Zhao, J. Li, Y. Sun, Prof. H. Cui, Prof. X. Xu,

College of Materials Science and Engineering, Ocean University of China, Qingdao 266100, China.

Dr. P. Murto

Department of Chemistry and Materials Science, Aalto University, Kemistintie 1, 02150 Espoo, Finland.

Dr. Z. Wang

Department of Materials Science and Metallurgy, University of Cambridge, Cambridge CB3 0FS, United Kingdom.

School of Engineering, College of Science and Engineering, University of Derby, Markeaton Street, Derby DE22 3AW, United Kingdom.

* Corresponding authors: X. Xu, email: xuxiaofeng@ouc.edu.cn

H. Cui, email: cuihongzhi@ouc.edu.cn

Z. Wang, email: z.wang@derby.ac.uk

Table of Contents

1. Materials

Sodium alginate (SA, 98%) and polyanionic cellulose (PAC, purity ≥ 96%, viscosity ≥ 50 mPa·s) were purchased from Shanghai Macklin Biochemical Co., Ltd, China. κ-carrageenan (κ-CA) was purchased from Beijing Mireida Technology Co., Ltd. Lithium chloride (LiCl, 98%), polyvinyl alcohol (PVA), and calcium chloride ($CaCl_2$, 99%) were purchased from Sinopharm Chemical Reagent Co., Ltd. [2-(methacryloyloxy)ethyl]dimethyl-(3-sulfopropyl) ammonium hydroxide (DMAPS), *N*-(2-Hydroxyethyl) acrylamide (HEAA, 98 wt%) were purchased from Zhengzhou Alfa Chemical Co., Ltd. Liquid paraffin was purchased from Tianjin Fuyu Fine Chemical Co., Ltd. Span-20 was purchased from Shandong Yusuo Chemical Technology Co., Ltd, China.

2. Material characterization

Water vapor sorption of all samples was evaluated in an artificial climate chamber (RGC-160D, Youke). Solid contents of inks were measured using a halogen moisture analyzer (METTLER TOLEDO, HC103). Rheological characterization was performed on the MCR 302e instrument. All tests were performed at 25 °C with a gap of 1 mm. The shear rate range for viscosity tests is 0.1 − 100 s^{-1}. The amplitude test has a fixed frequency of 1 Hz and a strain range of 0.1% to 100%. The shock test was performed at 1 Hz, alternating 120 s at 0.1% strain and 120 s at 100% strain. The Herschel-Bulkley computational model was used to simulate rheological behavior of SA HMP ink and predict the shear stress experience during printing. The related equations were solved in Matlab (MathWorks, Natick, MA). [1] The morphologies and elemental mapping were characterized by a scanning electron microscope (VEGA3, TESCAN) in combination with energy dispersive X-ray spectrometry. The tensile tests were performed using a universal mechanical testing system equipped digital force gauges (M5-100, Mark-10, accuracy: 0.02 N) and a force test stand (ESM 303, Mark-10). The UV−Vis−NIR absorption spectra were recorded

with LAMBDA 1050+ spectrometer equipped with an integrating sphere. The absorptance at each wavelength is defined by 1 − T − R, where T and R are the corresponding transmittance and reflectance, respectively. Raman spectra were measured via a spectrometer (alpha300, WITec).

3. Water vapor sorption characterization of SA

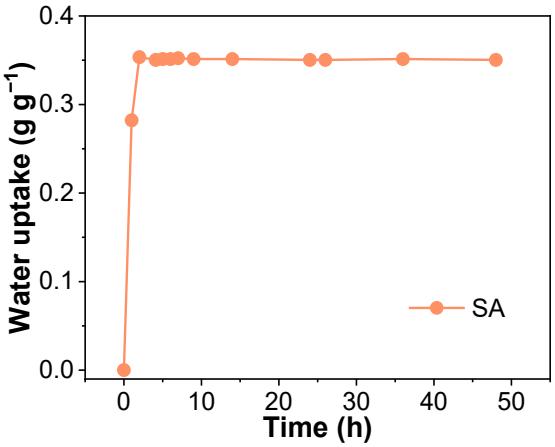

Figure S1. Water vapor sorption characterization under 90% RH and at 25 °C.

4. SA-HMP size characterization

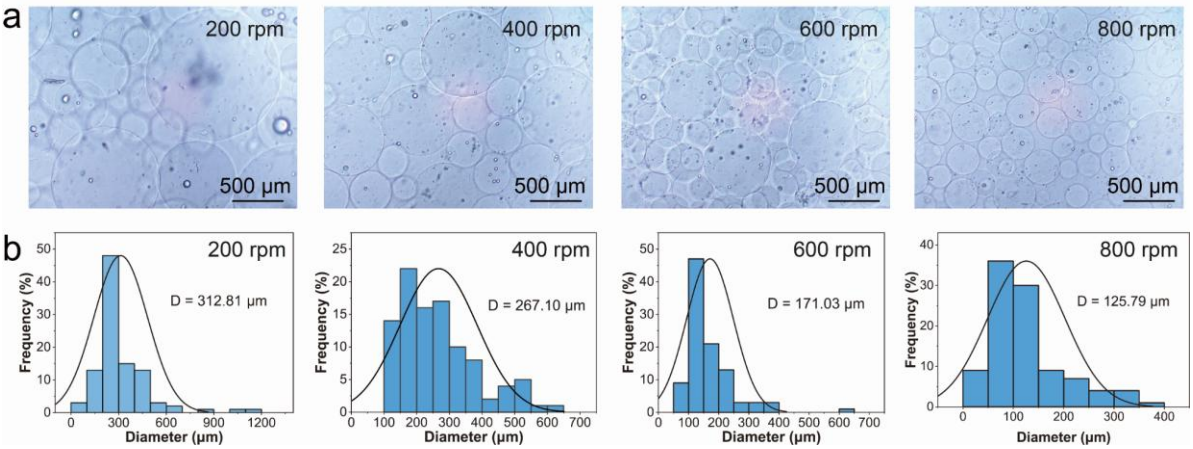

Figure S2. (a) Optical microscope images and (b) size distribution of SA-HMPs under different stirring speeds.

5. Mechanical strength evaluation

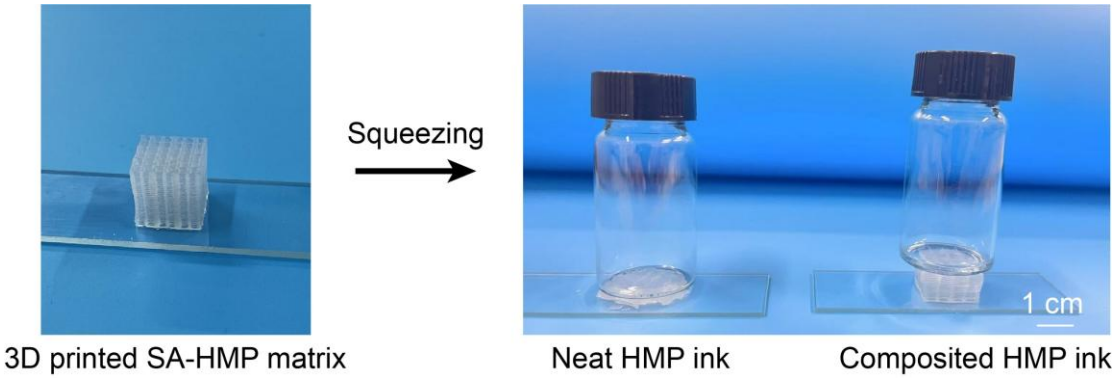

Figure S3. Mechanical strength characterization of 3D matrices based on SA-HMP inks without and with PDMAPS components.

6. Compression and tensile testing

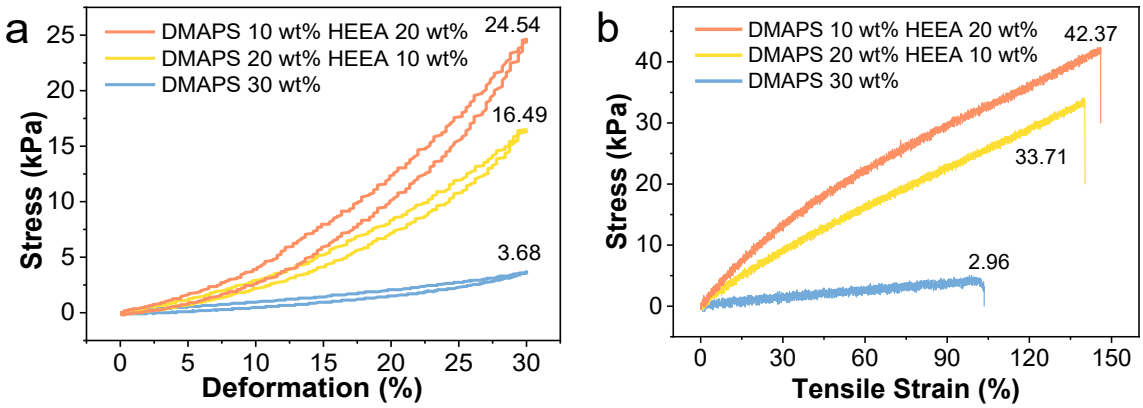

Figure S4. (a) Compression and (b) tensile tests of copolymer-based hydrogels.

7. Extrudability testing

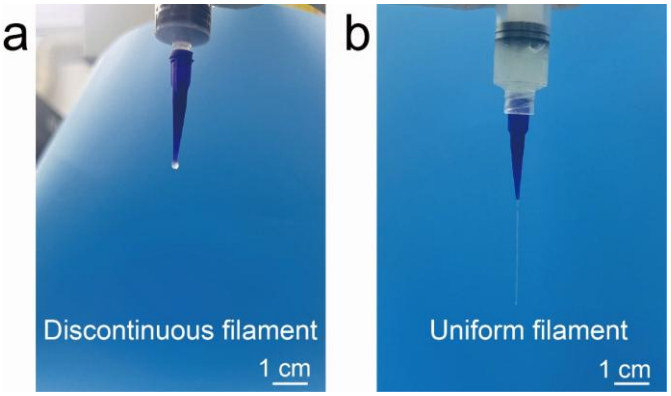

Figure S5. Extrudability tests of SA-HMP inks (a) without and (b) with PAC (Extrusion pressure: 8 psi).

8. Effect of LiCl concentrations on HMPs sizes

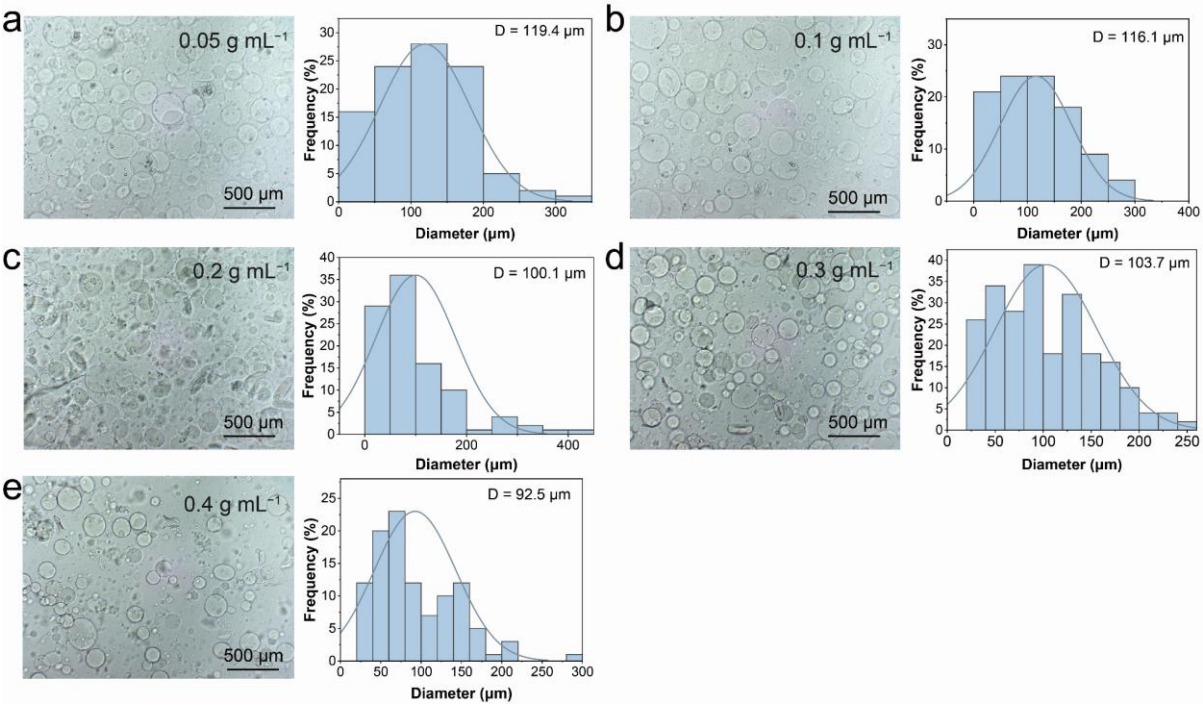

Figure S6. Optical microscope images and particle size distribution of HMPs with different LiCl concentrations: (a) 0.05 g mL^{-1}, (b) 0.1 g mL^{-1}, (c) 0.2 g mL^{-1}, (d) 0.3 g mL^{-1} and (e) 0.4 g mL^{-1}.

9. Effect of LiCl concentrations on ink extrudability

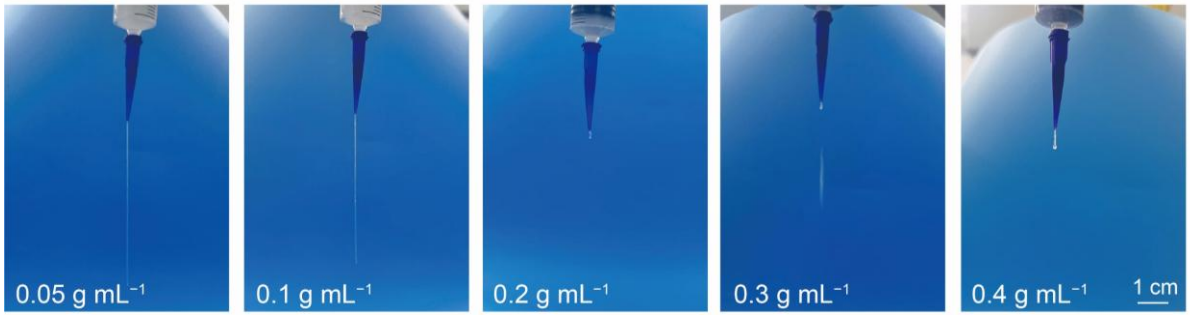

Figure S7. Extrudability tests of HMP inks with different LiCl concentrations (Extrusion Pressure: 8 psi).

10. Water vapor sorption characterization (I)

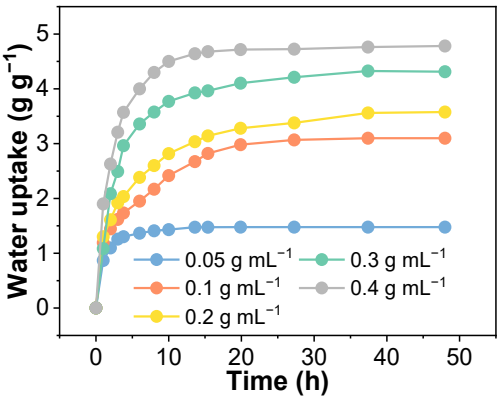

Figure S8. Water vapor sorption of SA-HMP filaments with different LiCl concentrations.

11. LiCl leakage evaluation

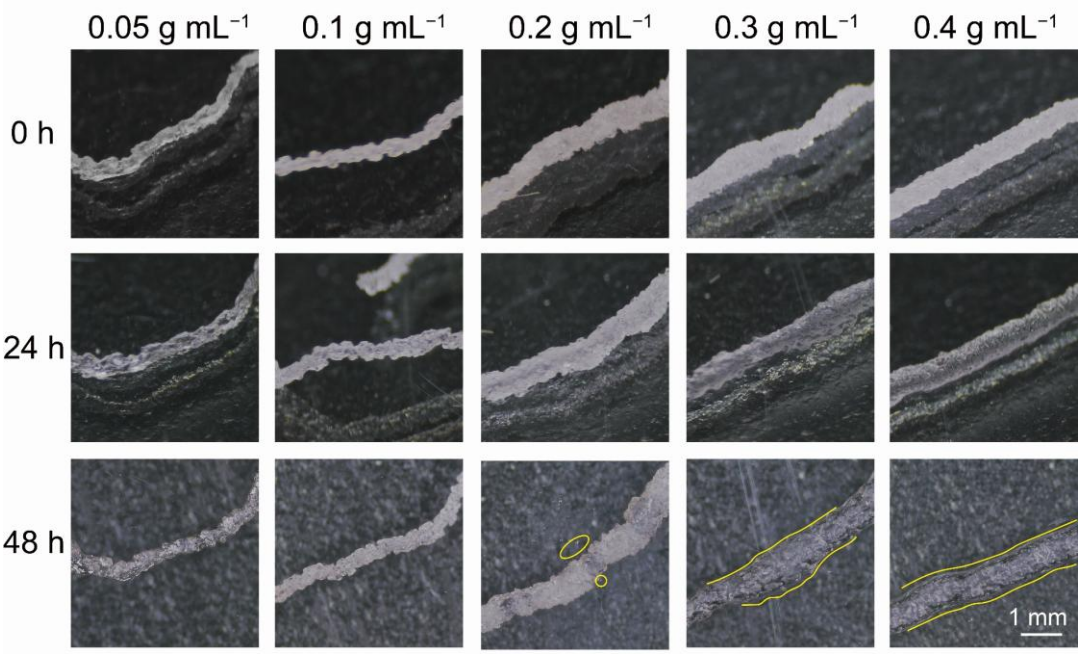

Figure S9. Optical photographs of printed filaments under 90% RH over time (yellow lines show LiCl solution leakage).

12. EDS mapping of filaments

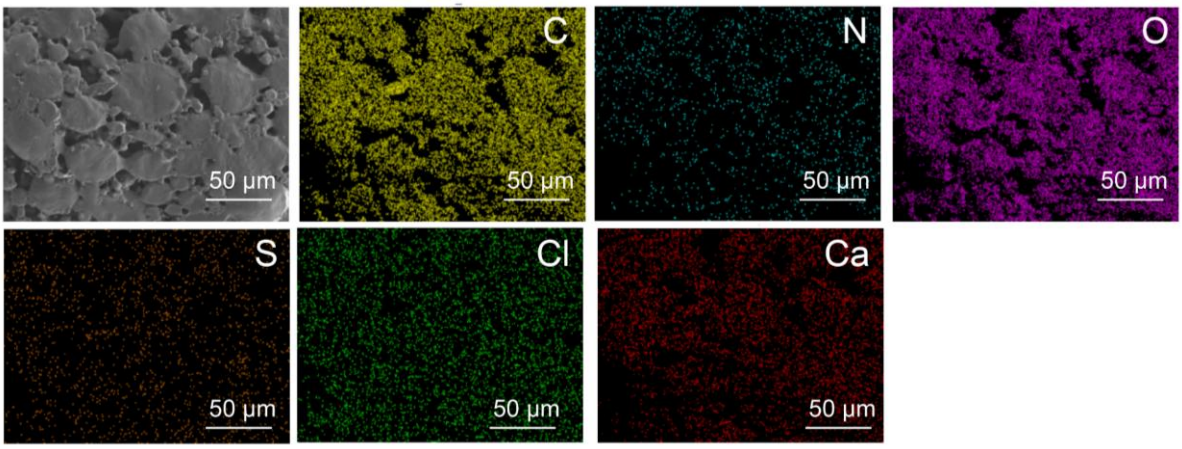

Figure S10. Distribution of C, O, N, S, Cl and Ca throughout printed SA-HMP filaments.

13. HMP jamming characterization

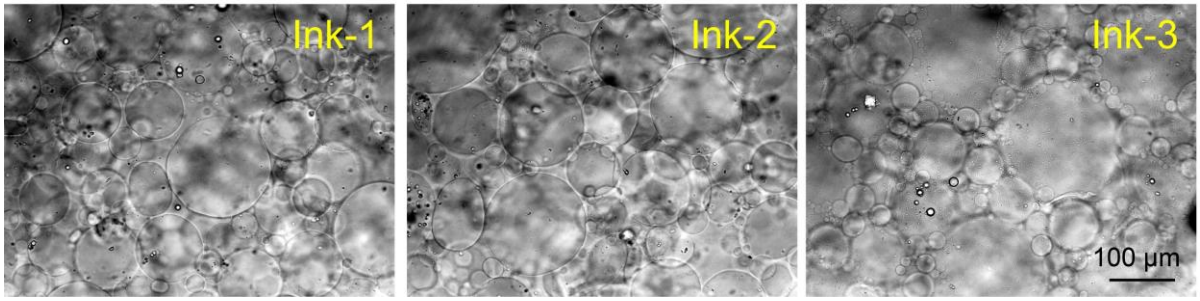

Figure S11. Optical microscope images of different inks.

14. Shear stress vs. shear rate

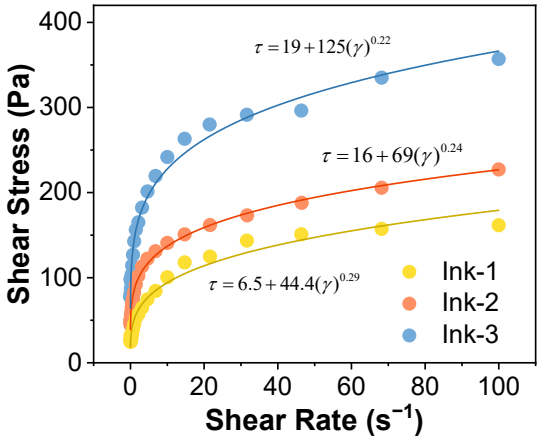

Figure S12. Correlations between shear stress and shear rate fitted using the Herschel-Bulkley Fluid model.

15. Shear-thinning characterization

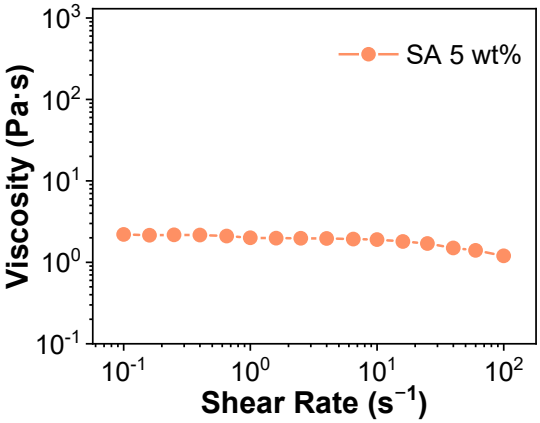

Figure S13. Shear viscosity versus shear rate of neat SA solutions across different shear rates.

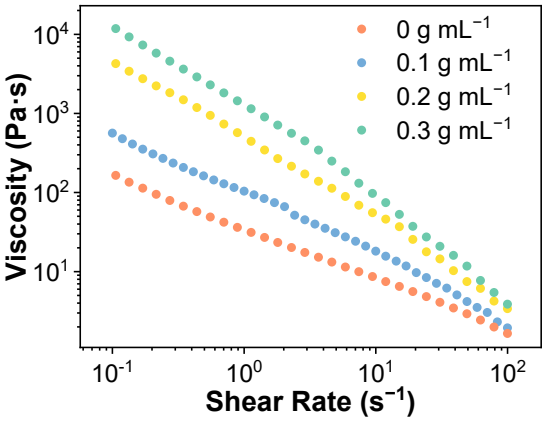

Figure S14. Shear viscosity versus shear rate of SA-HMP inks with varying LiCl concentrations.

16. Dynamic shear recovery measurements

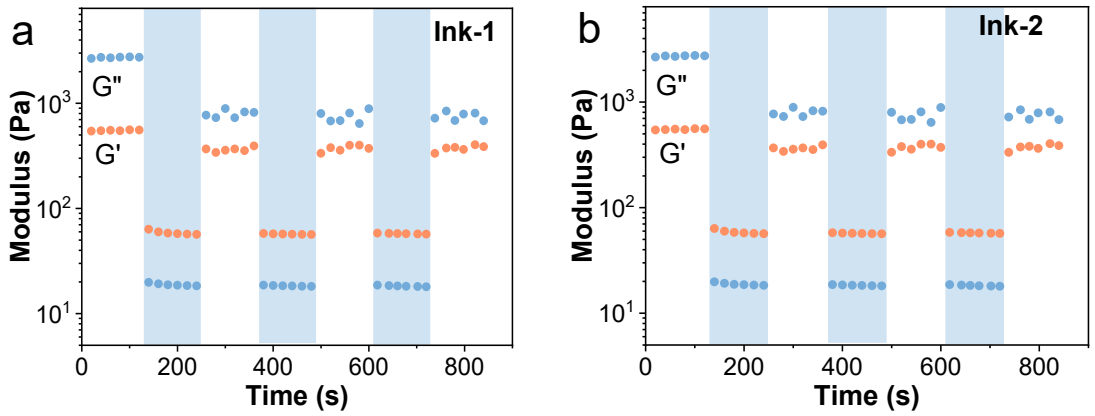

Figure S15. Shear recovery measurements under alternate low (1%) and high (100%) stains at a constant frequency of 1 Hz for (a) Ink-1 and (b) Ink-2.

17. Numerical simulations

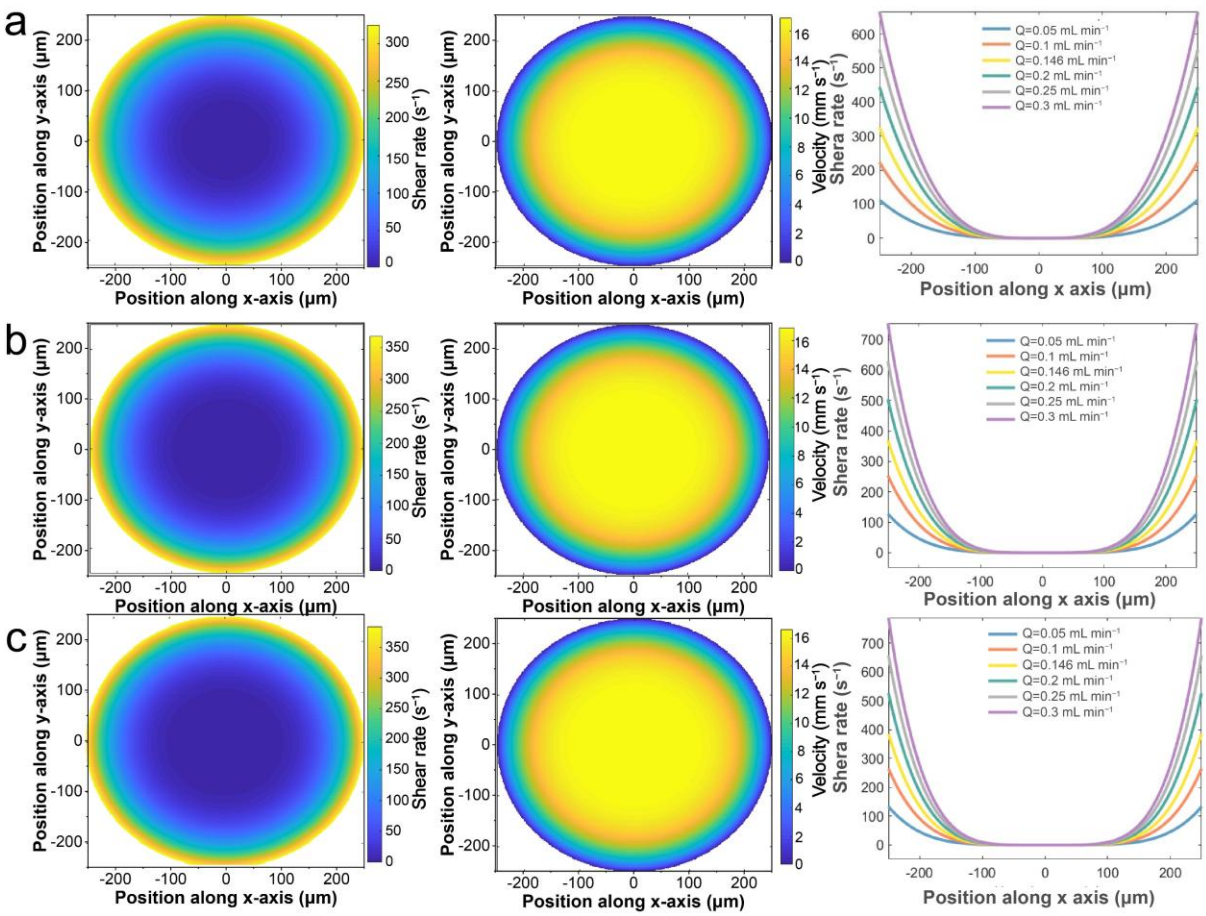

Figure S16. Rheological simulation of SA-HMP inks based on Herschel-Bulkley fluid model: (a) Ink-1, (b) Ink-2 and (c) Ink-3.

18. Printing precision characterization

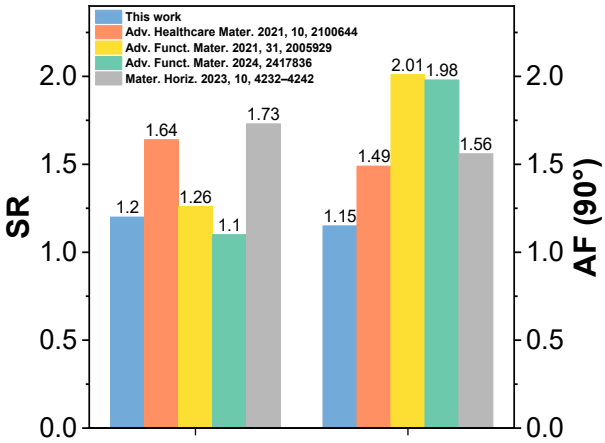

Figure S17. Summary of SR and AF (90°) values of representative microgel inks and Ink-3.

19. Sinking degree characterization

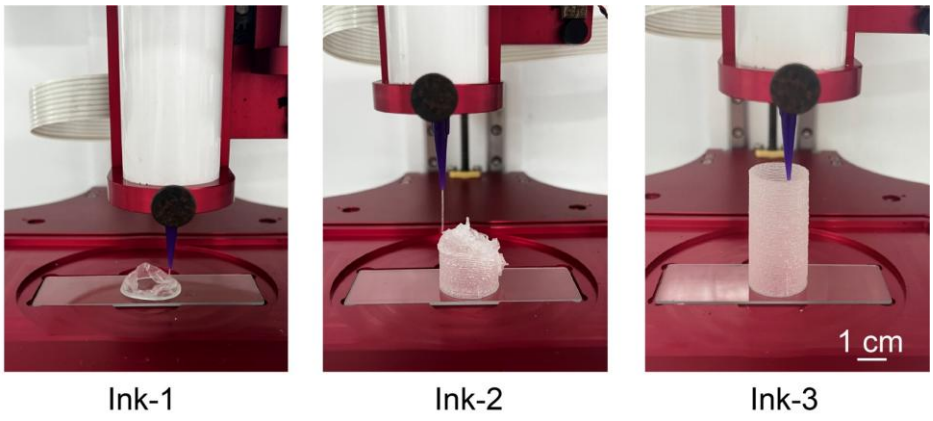

Figure S18. 3D-printed hollow cylinders using different inks.

20. Tensile testing for different printing directions

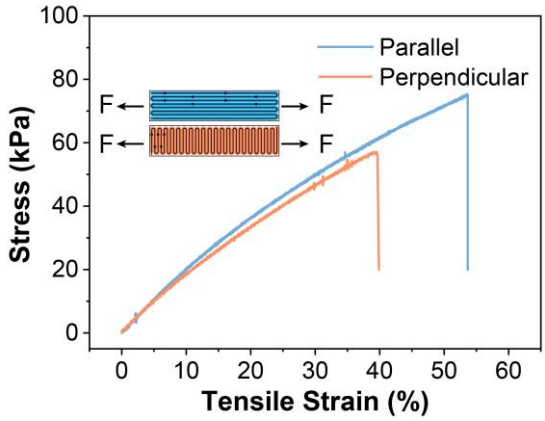

Figure S19. Tensile stress−strain curves for different printing directions.

21. Cyclic compression testing (I)

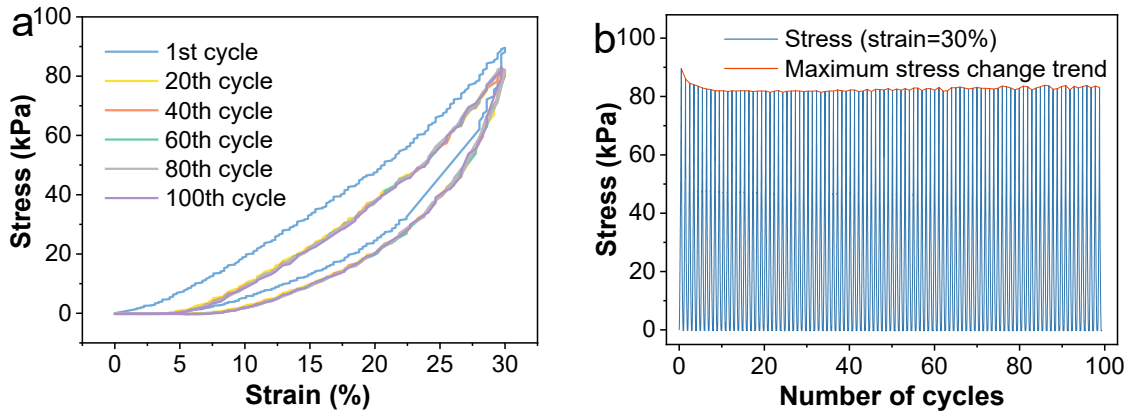

Figure S20. (a) Cyclic compressive stress−strain curves and (b) stress variations of 3D-printed structures using Ink-3 during loading−unloading (100 cycles) at a strain of 30%.

22. Compression characterization

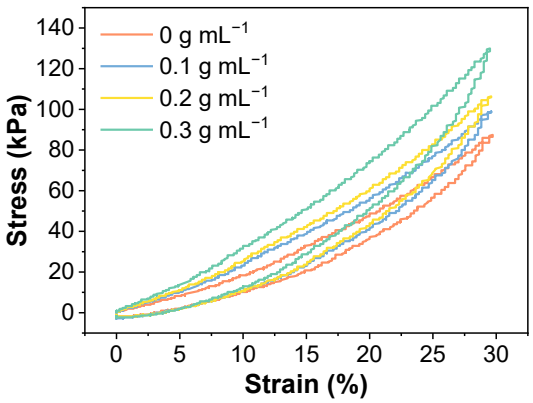

Figure S21. Compressive stress–strain curves of printed structures with varying LiCl concentrations under 30% strain.

23. Specific surface area characterization

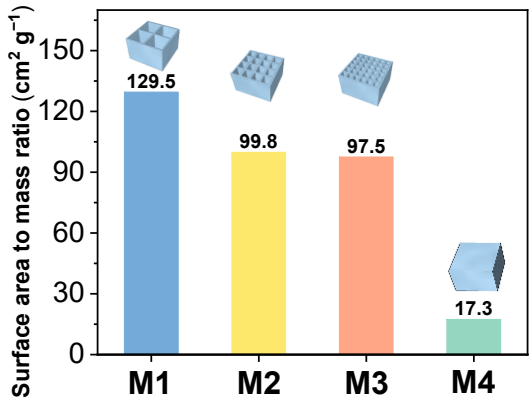

Figure S22. Specific surface areas of different 3D structures.

24. Water vapor sorption characterization (II)

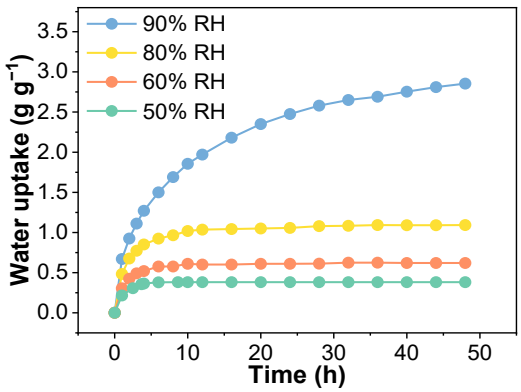

Figure S23. Water vapor sorption characterization under different RH levels.

25. Raman spectra

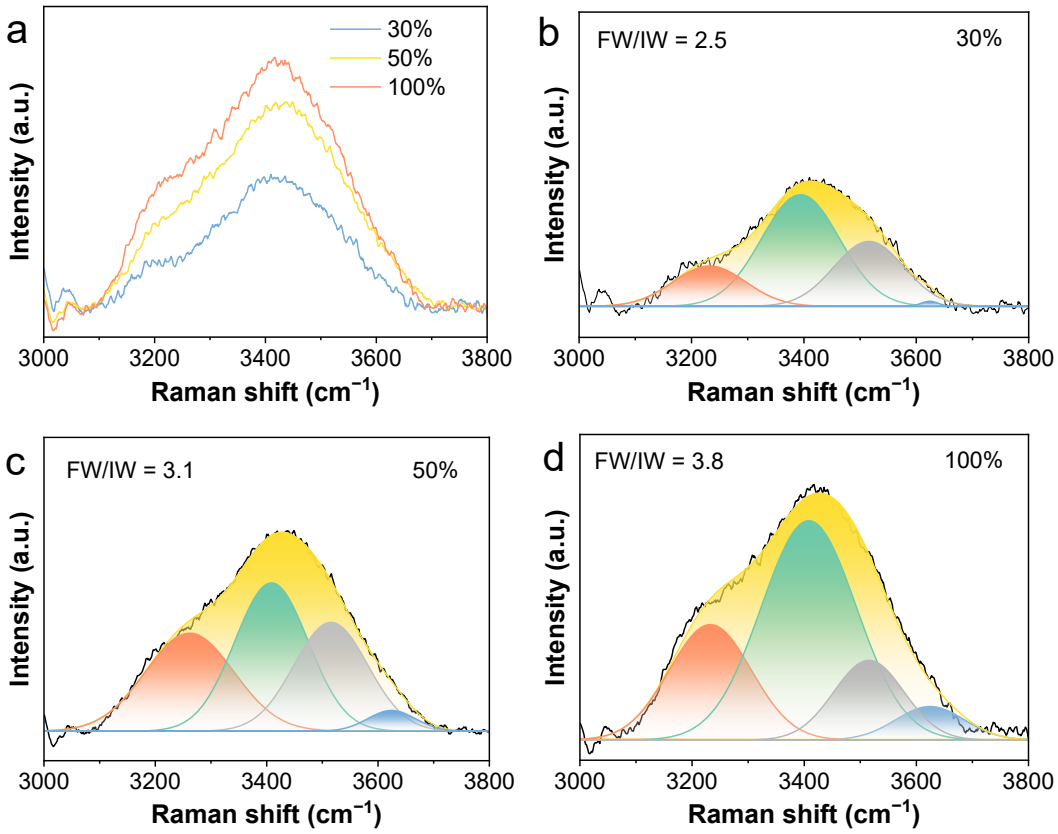

Figure S24. (a) Raman spectroscopic analysis of M2 during vapor sorption. Fitting peaks of intermediate water and free water with different water contents (b) 30% (c) 50% and (d) 100%.

26. Water desorption characterization (I)

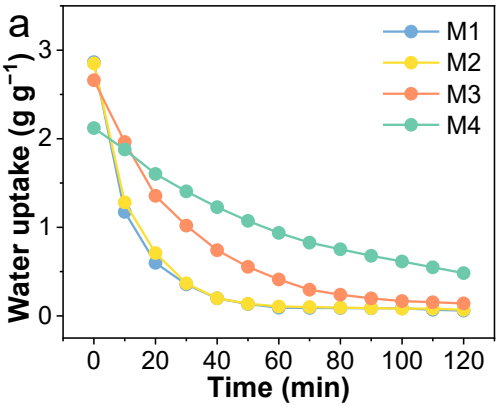

Figure S25. Water desorption characterization of M1−M4 at 80°C over time.

27. Cyclic sorption−desorption testing

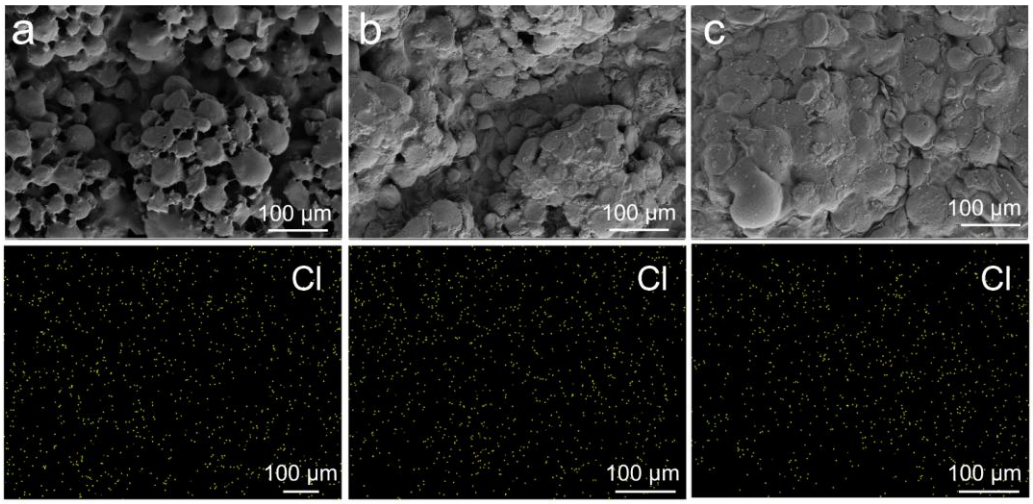

Figure S26. SEM images and EDS analysis of M2: (a) initial state, (b) after 1 sorption−desorption cycle, and (c) after 20 sorption−desorption cycles.

28. Rheological and mechanical properties of Ink-4

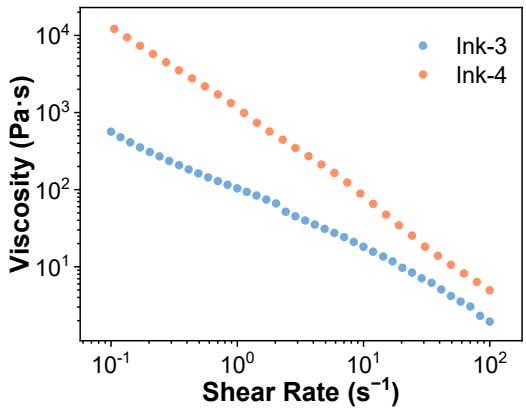

Figure S27. Shear viscosity versus shear rate for Ink-3 and Ink-4.

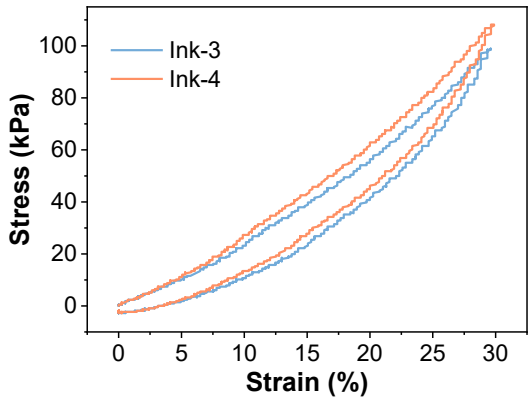

Figure S28. Compressive stress−strain curves of printed structures based on Ink-3 and Ink-4 under 30% strain.

29. EDS images of M5.

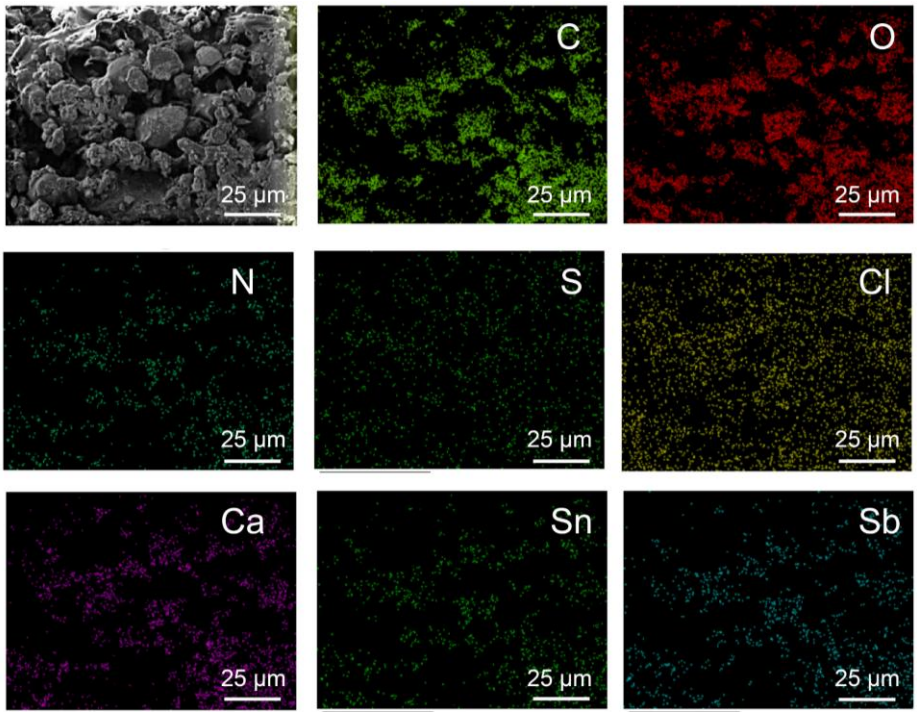

Figure S29. EDS images of M5.

30. Hygroscopic properties of M2 and M5

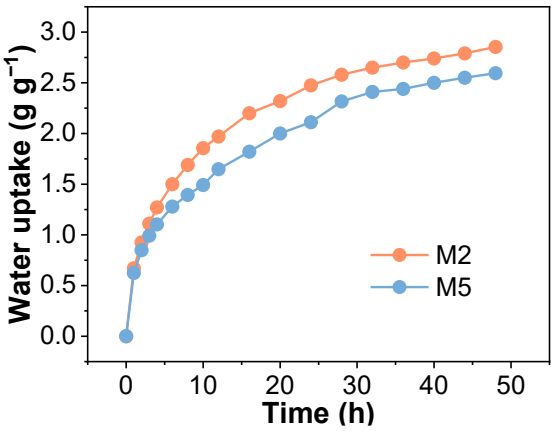

Figure S30. Water vapor sorption characterization of M2 and M5 under 90% RH and at 25 °C.

31. Summary of 3D-printable hygroscopic materials

Table S1. Summary of recently reported 3D-printed hygroscopic materials.

symbols[a]	years	hygroscopicity	conditions	materials	ref.
■	2021	0.41 g g^{-1}	20 °C, 40% RH	WPU/CNF/$CaCl_2$	[2]
●	2021	0.55 g g^{-1}	43% RH	CNF/$CaCl_2$	[3]
◆	2023	1.65 g g^{-1}	25 °C, 95% RH	CNF/LiCl	[4]
▼	2024	1.78 g g^{-1}	25 °C, 90% RH	Polymer	[5]
▲	2025	1.50 g g^{-1}	25 °C, 90% RH	Polymer/Glycerol	[6]
⬟	2025	1.80 g g^{-1}	25 °C, 88% RH	Polymer/LiCl	[7]
★	2025	2.85 g g^{-1}	25 °C, 90% RH	Polymer/LiCl	This work

[a] Corresponding to the labels in Figure 5f.

32. Dehumidification characterization

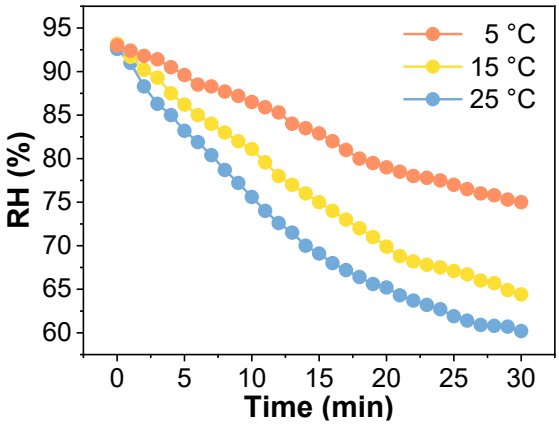

Figure S31. Dehumidification characterization across different temperatures.

33. Dew point calculation

The dew point (Ts) is calculated according to the Magnus-Tetens formula,[8]

$$Ts = \left(b \times \alpha\left(T, RH\right)\right) / \left(a - \alpha\left(T, RH\right)\right)$$

$$\alpha\left(T, RH\right) = ln\left(RH/100\right) + aT/\left(b+T\right)$$

where T_S is dew point (°C), T is the ambient temperature (°C), RH is the relative humidity of the air (%), and a and b are the Magnus coefficients, typically taken as a = 17.625 and b = 243.04 °C, respectively.

34. Water vapor sorption characterization (III)

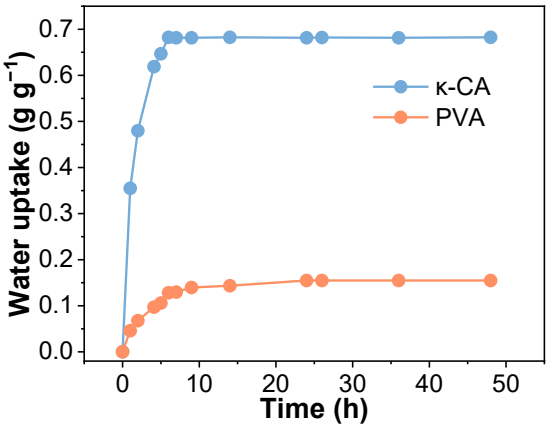

Figure S32. Water vapor sorption characterization of κ-CA and PVA under 90% RH and at 25 °C.

35. Size distribution of CA- and PVA-HMPs

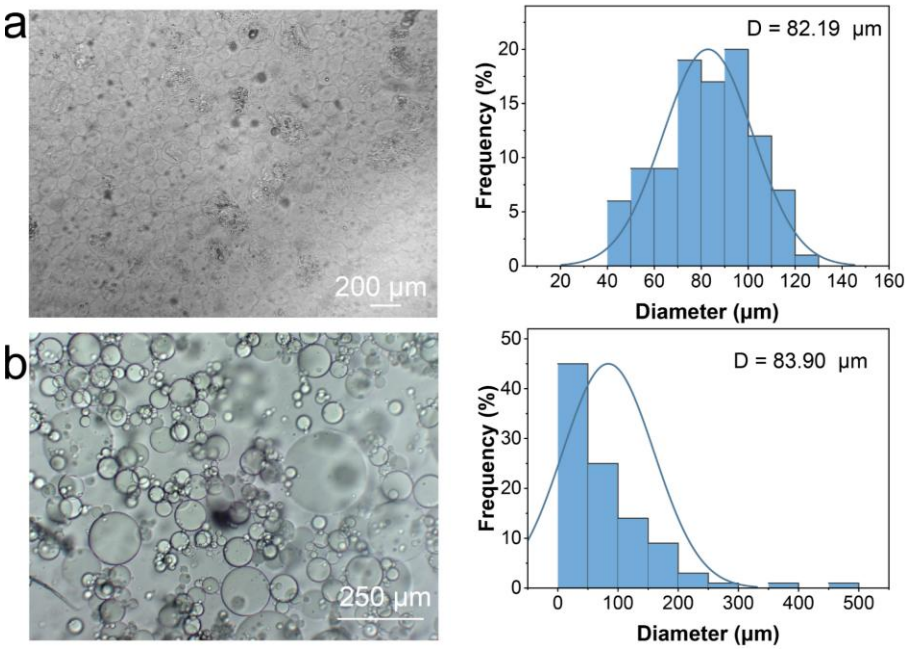

Figure S33. Optical microscopy images and average particle size of (a) CA-HMPs and (b) PVA-HMPs.

36. Dynamic recovery tests of CA-HMP and PVA-HMP inks

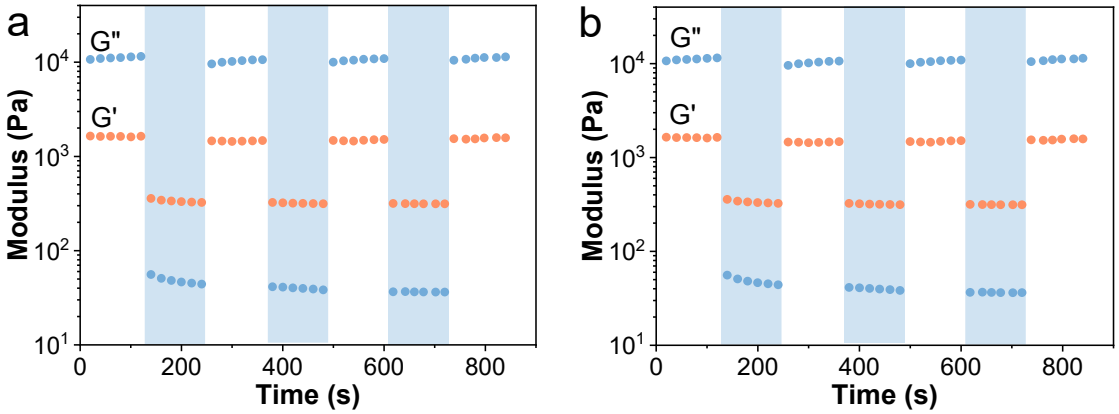

Figure S34. Shear recovery measurement under alternate low (1%) and high (100%) stains at a constant frequency of 1 Hz. for (a) CA-HMP ink and (b) PVA-HMP ink.

37. Cyclic compression testing (II)

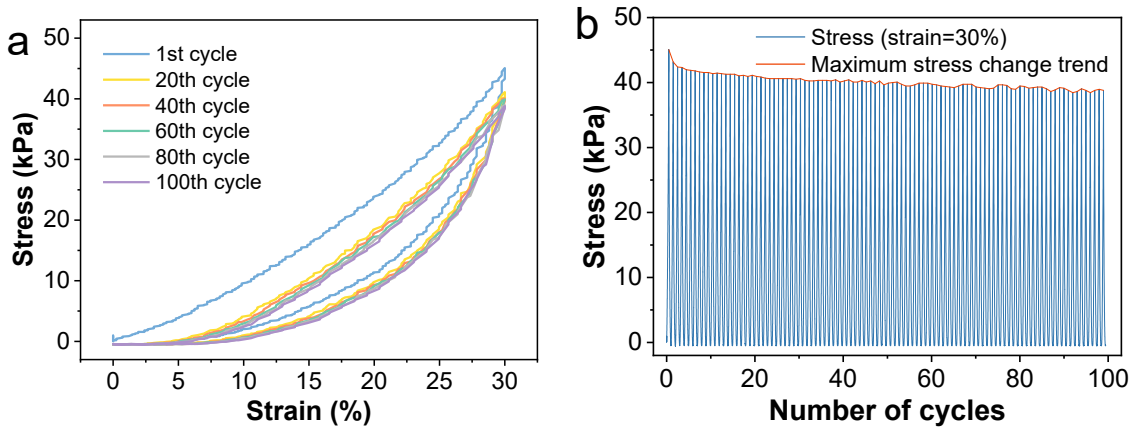

Figure S35. (a) Cyclic compressive stress−strain curves and (b) stress variations of CA-HMP printed hydrogel during loading−unloading (100 cycles) at a strain of 30%.

38. Cyclic compression testing (III)

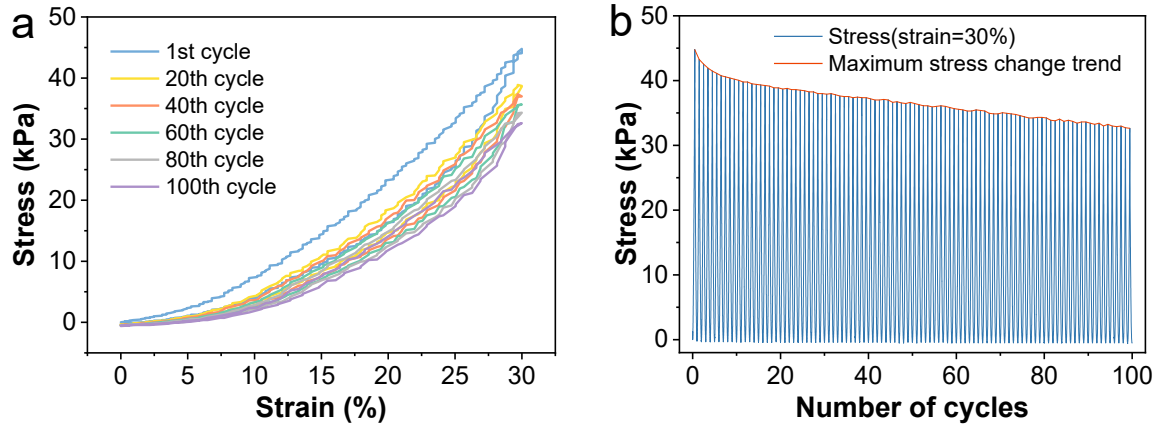

Figure S36. (a) Cyclic compressive stress−strain curves and (b) stress variations of PVA-HMP printed hydrogel during loading−unloading (100 cycles) at a strain of 30%.

39. Diameter changes of different filaments

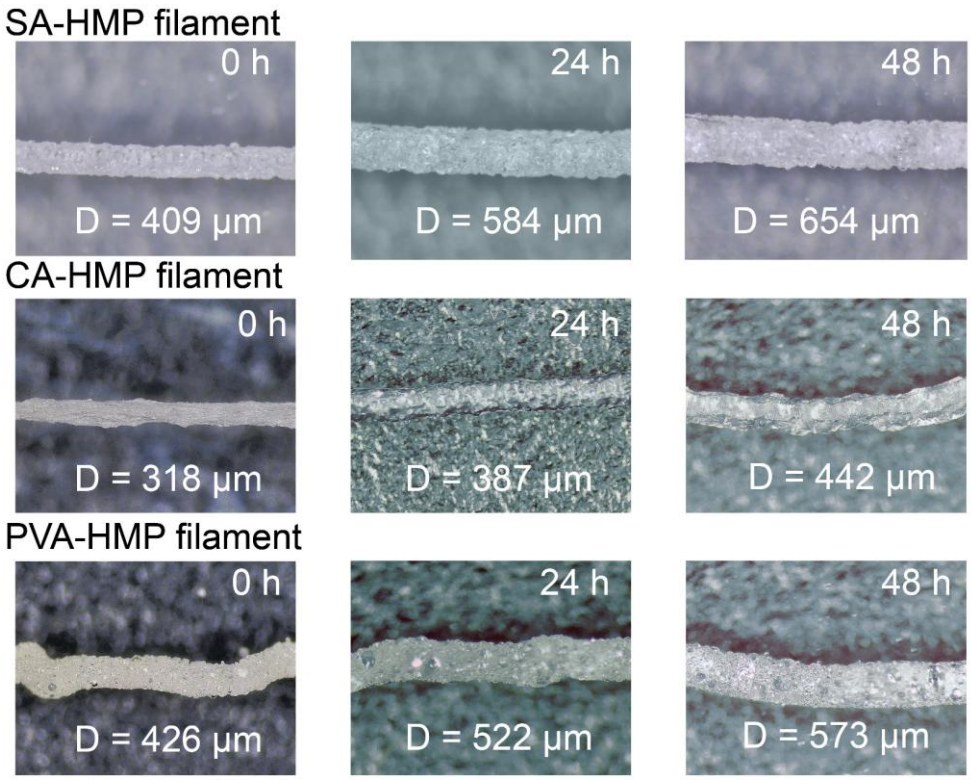

Figure S37. Diameter changes of different filaments during moisture sorption under 90% RH.

40. Water desorption characterization (II)

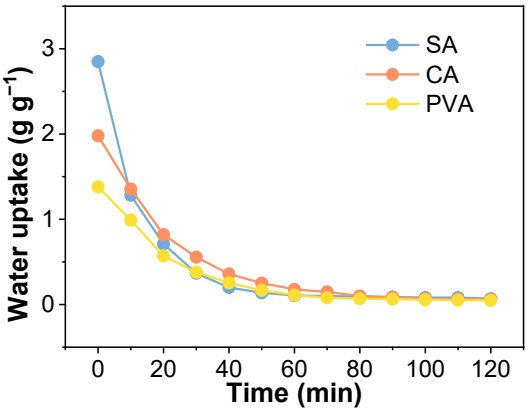

Figure S38. Water desorption characterization of 4×4 matrices based on SA-, CA- and PVA-HMP inks at 80 °C over time.

41. References

[1] D. Chimene, C. W. Peak, J. L. Gentry, J. K. Carrow, L. M. Cross, E. Mondragon, G. B. Cardoso, R. Kaunas, A. K. Gaharwar, *ACS Appl. Mater. Interfaces* **2018**, 10, 9957.

[2] Y. Chen, Z. Yu, H. Oguzlu, J. Jiang, M. Cho, M. Karaaslan, S. Renneckar, F. Jiang, *Addit. Manuf.* **2021**, 46, 102107.

[3] Y. Chen, Z. Yu, Y. Ye, Y. Zhang, G. Li, F. Jiang, *ACS Nano* **2021**, 15, 1869.

[4] P. Zhu, Z. Yu, H. Sun, D. Zheng, Y. Zheng, Y. Qian, Y. Wei, J. Lee, S. Srebnik, W. Chen, G. Chen, F. Jiang, *Adv. Mater.* **2023**, 36, 2306653.

[5] S. Li, K. Shao, X. Wu, S. Wang, J. Li, C. Guo, L. Yu, P. Murto, X. Xu, *Adv. Funct. Mater.* **2023**, 34, 2310020.

[6] Y. Wang, S. Li, J. Li, Y. Sun, Z. Li, P. Murto, Z. Wang, X. Xu, *J. Mater. Chem. A* **2025**, 13, 4413.

[7] Z. Chen, X. Yang, Q. Shao, R. Wang, *Adv. Funct. Mater.* **2025**, 2508512.

[8] M. G. Lawrence, *Bull. Am. Meteorol. Soc.* **2005**, 86, 225.